6

STATIC PROPERTIES

In previous chapters we have focused attention on the simulation itself, that is, on computing the phase-space trajectory for a system of model molecules. In this chapter we turn our attention to the analysis of computed trajectories. The analysis involves evaluating macroscopic properties—properties that pertain, not to individual molecules, but to an entire system of molecules.[†] The properties we consider in this chapter are thermodynamic quantities and static structure.

We divide thermodynamic properties into three classes: (1) simple functions of the Hamiltonian, (2) the thermodynamic response functions, which are derivatives of the simple functions, and (3) the entropy and free energies. Generally, as we move from class 1 to class 3, these properties become more difficult to evaluate accurately. We discuss the simple functions in Section 6.1, the response functions in Section 6.2, and the entropic properties in Section 6.3.

Static structure of matter can be measured by the radial distribution function $g(r)$, which describes the spatial organization of molecules about a central molecule. The function $g(r)$ plays a central role in the pair distribution function theory of dense fluids and provides a signature for identifying the lattice structure of crystalline solids. The radial distribution function can be simply evaluated from simulation data using the method developed in Section 6.4.

[†]W. Thomson, Lecture XVII, p. 167: "As to the physical properties of matter, which are more properly subjects of interest and the subjects that we occupy ourselves with...."

Throughout this chapter the following notation is used. For a system of N particles, the phase-space trajectory is represented by the set of numbers

$$\{[\mathbf{r}^N(k\Delta t), \mathbf{p}^N(k\Delta t)], k = 1, \ldots, M\}$$

Here $\mathbf{r}^N$ is the set of N position vectors and $\mathbf{p}^N$ is the set of N momentum vectors. The trajectory has been obtained from a simulation performed over M discrete times using the time-step Δt. From this trajectory the time average $\langle A \rangle$ of some function of the trajectory can be estimated by the sum

$$\langle A \rangle = \frac{1}{M} \sum_{k=1}^{M} A[\mathbf{r}^N(k\Delta t), \mathbf{p}^N(k\Delta t)] \tag{6.1}$$

As discussed in Section 2.6, the finite interval average (6.1) is an approximation to the infinite time average (2.41),

$$\langle A \rangle = \lim_{t \to \infty} \frac{1}{t} \int_{t_0}^{t_0 + t} A(\mathbf{r}^N, \mathbf{p}^N)\, d\tau$$

Dimensionless quantities are identified with an asterisk, as in Table 5.2.

6.1 SIMPLE THERMODYNAMIC PROPERTIES

The class of simple thermodynamic functions contains those properties that are obtained from averages of either the Hamiltonian or its spatial and momentum derivatives. The class contains several properties; however, in this section we discuss only temperature, internal energy, pressure, and mean-square force on a molecule. Other members of the class are of less general importance and are not discussed here; an example is the surface tension in Fowler's model of the vapor–liquid interface [1].

6.1.1 Internal Energy and Temperature

For an isolated system the total internal energy E is just the Hamiltonian $\mathscr{H}$,

$$E = \mathscr{H}(\mathbf{r}^N, \mathbf{p}^N) = \text{const} \tag{6.2}$$

which divides into a kinetic part E_k and a configurational part $\mathscr{U}$,

$$E = E_k + \mathscr{U} \tag{6.3}$$

As shown in Appendix C, the average kinetic energy is proportional to the

absolute temperature (2.43),

$$\langle E_k \rangle = \tfrac{3}{2}NkT = \frac{1}{2mM} \sum_{k=1}^{M} \sum_{i=1}^{N} \mathbf{p}_i(k\,\Delta t) \cdot \mathbf{p}_i(k\,\Delta t)$$

Here m is the mass of one particle. For soft spheres in a periodic system, the configurational internal energy is the average of the pair potential function $u(r)$,

$$U_c = \langle \mathscr{U} \rangle = \frac{1}{M} \sum_{k=1}^{M} \sum_{\boldsymbol{\alpha}} \sum\sum_{i<j} u\left[\left|\mathbf{r}_{ij}(k\,\Delta t) - \boldsymbol{\alpha} L\right|\right] \tag{6.4}$$

Recall u is a two-body potential, such as the Lennard-Jones model (5.4), $r_{ij} = |\mathbf{r}_i - \mathbf{r}_j|$ is the scalar distance between the centers of atoms i and j, L is the length of one edge of the primary cell, and $\boldsymbol{\alpha}$ is the cell translation vector of Section 2.9.

Long-Range Corrections. Often in soft-sphere simulations we use a truncated pair potential (see Section 5.1.1), but we want property values for the full untruncated potential. In those situations, an expression such as (6.4) is incomplete because the simulation ignores interactions between atoms separated by distances greater than the cutoff distance r_c. Therefore, simulation results for $\langle \mathscr{U} \rangle$ must be corrected by adding an estimate for the long-range contribution U_{LR}. The estimation is done in the following way.

In the classical statistical mechanics of atomic, pairwise additive substances, the configurational internal energy U_c can be written [2, 3] as an integral over the pair potential $u(r)$ weighted with the radial distribution function $g(r)$,

$$\frac{U_c}{N} = 2\pi\rho \int_0^\infty u(r)\, g(r)\, r^2\, dr \tag{6.5}$$

where $\rho = N/V$ is the number density. The integral in (6.5) can be divided as

$$\frac{U_c}{N} = 2\pi\rho \int_0^{r_c} u(r)\, g(r)\, r^2\, dr + 2\pi\rho \int_{r_c}^\infty u(r)\, g(r)\, r^2\, dr \tag{6.6}$$

The first term on the rhs of (6.6) is just $\langle \mathscr{U} \rangle / N$, which is evaluated from a molecular dynamics simulation via (6.4). The second term in (6.6) is the long-range correction. Therefore, the complete expression for the configura-

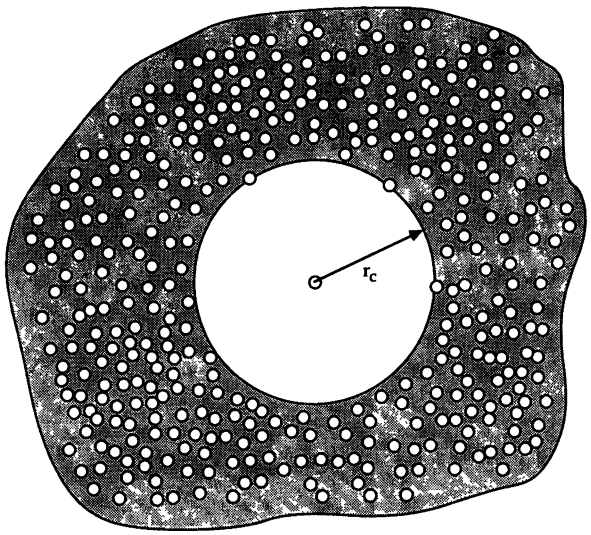

FIGURE 6.1 Simulation provides only a portion of most thermodynamic properties. During a simulation we obtain contributions to properties that arise from interactions between a central atom and others lying within a radius r_c. Contributions from beyond r_c are typically estimated using a mean-field approximation: we assume outlying atoms are uniformly distributed about the central atom and therefore present a small, constant contribution to thermodynamic properties.

tional internal energy is

$$\frac{U_c}{N} = \frac{\langle \mathscr{U} \rangle}{N} + U_{\text{LR}} \tag{6.7}$$

In the absence of data for $g(r)$ for $r > r_c$, the long-range correction is typically estimated by

$$U_{\text{LR}} = 2\pi\rho \int_{r_c}^{\infty} u(r) r^2 \, dr \tag{6.8}$$

That is, the substance is assumed to be uniform $[g(r) = 1]$ beyond the potential cutoff distance r_c. This amounts to a mean-field approximation for the long-range portion of the internal energy; see Figure 6.1. For the Lennard-Jones potential the integral in (6.8) can be performed analytically, resulting in

$$U^*_{\text{LR}} = \frac{8\pi\rho^*}{3(r_c^*)^3}\left(\frac{1}{3(r_c^*)^6} - 1\right) \approx \frac{-8\pi\rho^*}{3(r_c^*)^3} \tag{6.9}$$

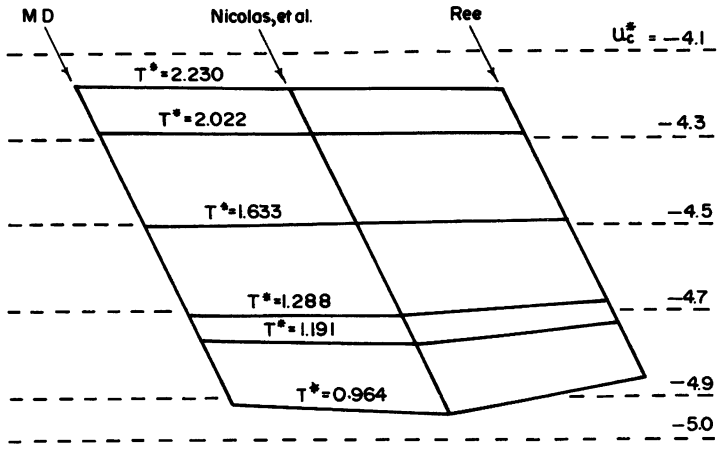

FIGURE 6.2 Tests of Ree and Nicolas et al. equations of state for the configurational internal energy U_c^* of the Lennard-Jones fluid at $\rho^* = 0.7$. The simulation results are from runs using 256 atoms and 500,000 time-steps and have statistical uncertainties of $\Delta U^* \leq 0.002$ at the 95% confidence level.

Thus, at a fixed number density, the long-range correction is merely a constant that is added to a molecular dynamics result for $\langle \mathscr{U}^* \rangle$.

If the shifted-force potential (5.12) is used in a simulation and if results are desired for the original unshifted potential, then corrections for the shift are needed. However, since the shifted-force potential is useful for testing code, not for making production runs, the expressions for the corrections are not given here (they may be found elsewhere [4]).

Sample Results. Figure 6.2 shows molecular dynamics results for U_c^* computed for the Lennard-Jones fluid at a density $\rho^* = 0.7$. The simulations were done using 256 atoms and the pair potential truncated at $r_c^* = 2.5$. Each run was started from an fcc lattice and each was continued for up to 500,000 time-steps. Runs at low temperatures used a time-step $\Delta t^* = 0.004$, while at high temperatures $\Delta t^* = 0.003$. Averages for properties were computed by stratified systematic sampling at intervals of 50 time-steps, and statistical uncertainties in U_c^* were computed to be $\Delta U^* \leq 0.002$ at the 95% confidence level. Over the temperature range $0.96 < T^* < 2.23$, the values of U_c^* at $\rho^* = 0.7$ are accurately represented by the cubic

$$U_c^* = -5.6597 + 0.8893T^* - 0.13588T^{*2} + 0.015593T^{*3} \qquad (6.10)$$

A quadratic in temperature will fit the U-data equally well, but this cubic provides more reliable values for the residual isometric heat capacity (see Section 6.2.1).

Figure 6.2 uses a two-way plot (see Appendix D) to compare these simulation results with U_c-values provided by empirical equations of state

given by Nicolas et al. [4] and by Ree [5]. Both empirical equations are based on fits to collections of Lennard-Jones simulation data. At the density and temperatures studied here, both correlations reproduce U_c within 1% of nearly all our simulation values, though the Ree equation consistently provides less negative values of U_c than found in the simulation. The discrepancies are largest at the lowest temperatures. A careful inspection of Figure 6.2 leads us to anticipate that both correlations will reliably estimate the residual heat capacity $[C_v^R = (\partial U_c / \partial T)_v]$ at high temperatures, but at low temperatures the Ree equation will underestimate C_v^R, while the Nicolas et al. equation will overestimate C_v^R.

6.1.2 Pressure

The pressure P is related to molecular quantities through the virial equation of state, which is derived in Appendix B,

$$\frac{P}{\rho kT} = 1 - \frac{1}{3NkT}\left\langle \sum\sum_{i<j} r_{ij}\frac{du(r_{ij})}{dr_{ij}} \right\rangle \tag{6.11}$$

The first term on the rhs is the ideal-gas contribution, and the second term accounts for intermolecular forces, assuming a pairwise additive potential $u(r)$. In periodic systems, (6.11) can be evaluated from a phase space trajectory via

$$\frac{P_{\text{md}}}{\rho kT} = 1 - \frac{1}{3MNkT}\sum_{k=1}^{M}\sum_{\boldsymbol{\alpha}}\sum\sum_{i<j}|\mathbf{r}_{ij}(k\,\Delta t) - \boldsymbol{\alpha}L|\frac{du\left[|\mathbf{r}_{ij}(k\,\Delta t) - \boldsymbol{\alpha}L|\right]}{dr_{ij}} \tag{6.12}$$

Here L is the length of one edge of the primary cell and $\boldsymbol{\alpha}$ is the cell translation vector discussed in Section 2.9.

Just as for the internal energy, when a truncated potential is used, a long-range correction must be added to the molecular dynamics result for the virial. Thus the full expression for the pressure is

$$P = P_{\text{md}} + P_{\text{LR}} \tag{6.13}$$

The long-range correction can be estimated by a procedure analogous to that described above for the internal energy. The result is

$$\frac{P_{\text{LR}}}{\rho kT} = \frac{-2\pi\rho}{3kT}\int_{r_c}^{\infty} r\frac{du(r)}{dr}g(r)r^2\,dr \tag{6.14}$$

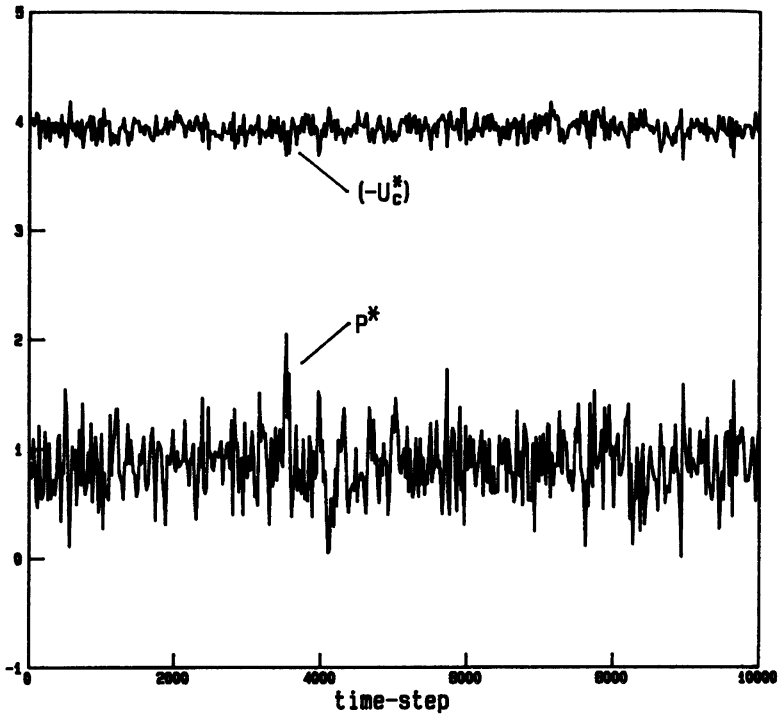

FIGURE 6.3 Fluctuations in the instantaneous pressure $P^* = P\sigma^3/\varepsilon$ are usually larger than those in the instantaneous configurational internal energy $\mathscr{U}^* = \mathscr{U}/N\varepsilon$. (Note that $-\mathscr{U}^*$ is plotted here.) These results are from a molecular dynamics simulation of 108 Lennard-Jones atoms at $\rho^* = 0.6$, $\langle T^* \rangle = 1.542$. Values are plotted here at intervals of 20 time-steps; the time-step was $\Delta t^* = 0.004$.

Assuming $g(r) = 1$ and applying (6.14) to the Lennard-Jones model, we find

$$\frac{P^*_{\mathrm{LR}}}{\rho^* T^*} = \frac{-16\pi\rho^*}{3T^*(r_c^*)^3}\left(1 - \frac{2}{3(r_c^*)^6}\right) \approx \frac{-16\pi\rho^*}{3T^*(r_c^*)^3} \tag{6.15}$$

which is again merely a constant to be added to the simulation result.

For soft spheres at liquid densities, the pressure exhibits larger fluctuations than does the internal energy; an example is provided in Figure 6.3. These large fluctuations occur because $r\,du/dr$ usually changes more quickly with r than does the potential $u(r)$. That is, for most pair separations

$$\left|\frac{d}{dr}\left(r\frac{du}{dr}\right)\right| > \left|\frac{du}{dr}\right| \tag{6.16}$$

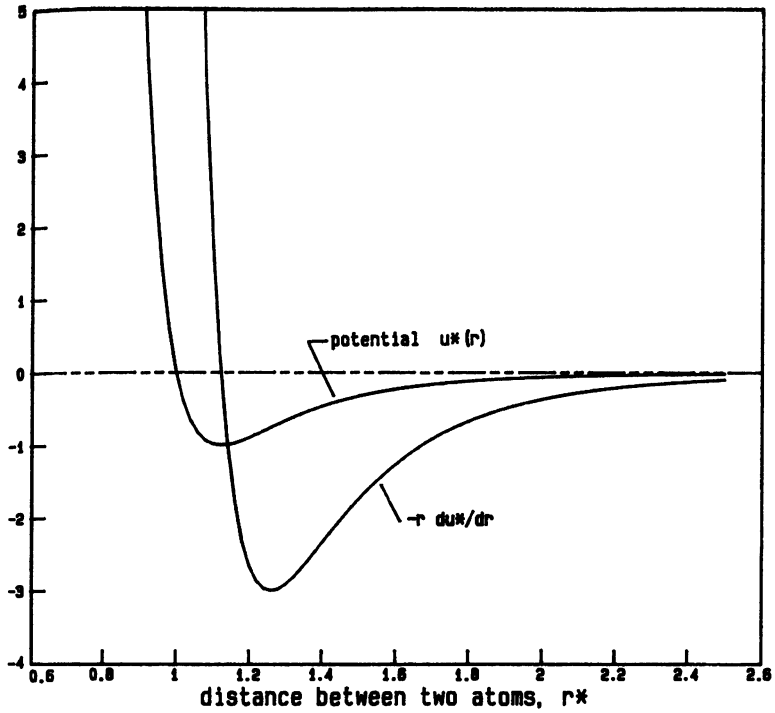

FIGURE 6.4 For the Lennard-Jones (12, 6) potential the magnitude of the slope of $\{-r^* du^*/dr^*\}$ is nearly everywhere greater than the magnitude of the slope of $u^*(r^*)$; therefore, fluctuations in the instantaneous pressure are larger than those in the internal energy, as shown in Figure 6.3.

For the Lennard-Jones (12,6) potential, the inequality in (6.16) is violated only for pair separations near the minimum in $(-r\,du/dr)$; specifically, for

$$1.2445 \leq r^* \leq 1.2801 \tag{6.17}$$

Otherwise, Figure 6.4 shows that for any small change in r, the magnitude of the slope of $r\,du/dr$ is nearly everywhere greater than that of $u(r)$.

Molecular dynamics results for the residual pressure,

$$P_{\text{res}} = P - \rho kT \tag{6.18}$$

are shown in Figure 6.5 for the Lennard-Jones fluid at $\rho^* = 0.7$. These results are from the same simulations that gave the U_c results in Figure 6.2. The statistical uncertainties are $\Delta P^*_{\text{res}} \leq 0.006$ at the 95% confidence level. Over the temperature range $0.96 < T^* < 2.23$, values of the residual pressure are

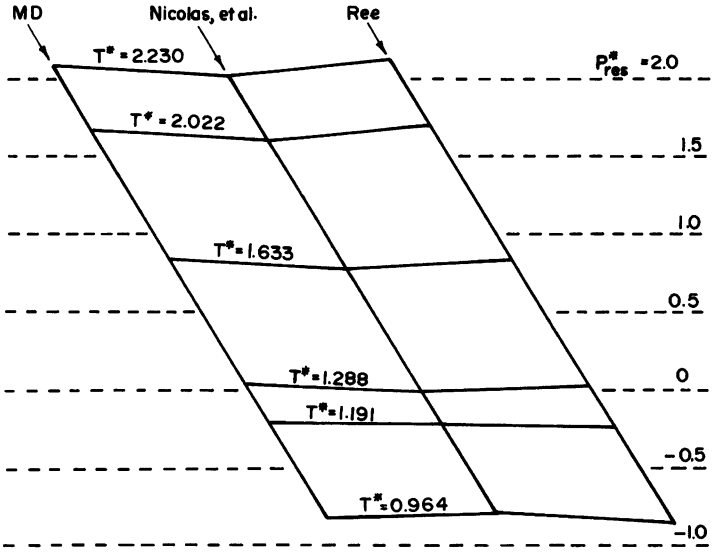

FIGURE 6.5 Tests of Ree and Nicolas et al. equations of state for the residual pressure P^*_{res} of the Lennard-Jones fluid at $\rho^* = 0.7$. Simulation results are from the runs described in Section 6.1.1 for U_c. The statistical uncertainties in these simulation results are $\Delta P^*_{res} \leq 0.006$ at the 95% confidence level.

accurately represented by

$$P^*_{res} = -4.1687 + 4.2808T^* - 0.9635T^{*2} + 0.1360T^{*3} \tag{6.19}$$

Note that for the Lennard-Jones substance P_{res} and U_c are related by

$$P^* - \rho^* T^* = 2\rho^* \left[U_c^* + 4\langle r^{*-12} \rangle \right] \tag{6.20}$$

where $\langle r^{*-12} \rangle$ is the time average per atom of the repulsive part of the potential.

Simulation results for the pressure of the Lennard-Jones substance have been fit by Nicolas et al. [4] and by Ree [5] to empirical equations in density and temperature. The 33-parameter Nicolas et al. equation applies to states in the region $\{0 \leq \rho^* \leq 1.2\}$ and $\{0.5 \leq T^* \leq 6\}$, while the 15-parameter Ree equation is restricted to states in $\{0.05 \leq \rho^* \leq 0.96\}$ and $\{0.76 \leq T^* \leq 2.698\}$. A third empirical equation has been devised by Adachi et al. [6]. With these equations any thermodynamic property may be computed by invoking the appropriate thermodynamic relation.

At the density shown in Figure 6.5 ($\rho^* = 0.7$), tests of the empirical equations indicate that the absolute deviations in the residual pressure are no more than 0.08 for the Nicolas et al. equation [4] and no more than 0.04

for the Ree equation [5]. Except at the lowest temperature, the Nicolas et al. equation consistently underestimates P_{res}. In contrast, at high temperatures the Ree equation overestimates P_{res} but at low temperatures it underestimates P_{res}.

6.1.3 Mean-Square Force

The mean-square force $\langle F^2 \rangle$ on an atom gives information about the shape of the repulsive part of the intermolecular pair potential. It is both the zero-time limit of the force autocorrelation function and the second frequency moment of the Fourier transform of the velocity autocorrelation function [7]. Experimentally, $\langle F^2 \rangle$ can be obtained from vapor–liquid isotopic separation factors [8–10].

Two methods are available for analyzing simulation data for $\langle F^2 \rangle$. The direct method is to form the time-average square of the force on, say, atom 1,

$$\langle F_1^2 \rangle = \left\langle \sum_{j \neq 1} \left(\nabla u(r_{1j}) \right)^2 \right\rangle \tag{6.21}$$

The symbol ∇ is the gradient operator, $\nabla \equiv \partial / \partial \mathbf{r}$. The statistical precision of the result can be improved by averaging over $\frac{1}{2}N$ unique atomic origins rather than just atom 1. Then interpreting the time average in (6.21) in the usual way, the expression for the mean-square force in periodic systems becomes

$$\langle F^2 \rangle = \frac{2}{MN} \sum_{k=1}^{M} \sum_{\alpha} \sum\sum_{i<j} \left(\nabla u \left[\left| \mathbf{r}_{ij}(k \, \Delta t) - \alpha L \right| \right] \right)^2 \tag{6.22}$$

The second method for evaluating $\langle F^2 \rangle$ is obtained from the identity [7, 11]

$$\left\langle W(\mathbf{r}^N) \nabla \mathscr{U}(\mathbf{r}^N) \right\rangle = kT \left\langle \nabla W(\mathbf{r}^N) \right\rangle \tag{6.23}$$

where W is any regular function of the atomic positions and $\mathscr{U}$ is the full potential energy function. For the mean-square force, we use $W = \nabla \mathscr{U}$, so

$$\langle F^2 \rangle = \left\langle \left(\nabla \mathscr{U}(\mathbf{r}^N) \right)^2 \right\rangle = kT \left\langle \nabla^2 \mathscr{U}(\mathbf{r}^N) \right\rangle \tag{6.24}$$

where $\nabla^2 \equiv \partial^2 / \partial \mathbf{r}^2$ is the Laplacian operator.† The working expression for

†W. Thomson, Lecture X, p. 98: "I took the liberty of asking Prof. Ball two days ago whether he had a name for this symbol ∇^2; and he has mentioned to me *nabla*, a humorous suggestion of Maxwell's. It is the name of an Egyptian harp which was of that shape. I do not know that it is a bad name for it. Laplacian I do not like for several reasons both historical and phonetical." Lecture XIII, p. 128: "I have another name from Prof. Ball for ∇, which is *atled*, or *delta* spelt backwards."

$\langle F^2 \rangle$ is now

$$\langle F^{*2} \rangle = \frac{2T^*}{MN} \sum_{k=1}^{M} \sum_{\alpha} \sum\sum_{i<j} \left(\nabla^2 u^* \left[\left| \mathbf{r}_{ij}^*(k\,\Delta t) - \alpha L^* \right| \right] \right) \tag{6.25}$$

Even for the Lennard-Jones potential the Laplacian is tedious to evaluate, but after some effort we find [12]

$$\nabla^2 u^* = 24(22r^{*-14} - 5r^{*-8}) \tag{6.26}$$

In using (6.22) we must not forget the long-range correction that applies to the simulation results for truncated potentials. If (6.25) is used, the long-range correction may be small and safely neglected. Thus for the Lennard-Jones model, the correction to (6.25) varies as r_c^{-5}, and for $r_c \geq 2.5\sigma$, the correction is negligible.

6.2 THERMODYNAMIC RESPONSE FUNCTIONS

The response functions reveal how simple thermodynamic quantities respond to changes in measurables, usually either the pressure or temperature. Hence they are derivative quantities. To cite a particular example, the constant-volume heat capacity measures how the internal energy responds to an isometric change in temperature,

$$C_v = \left(\frac{\partial E}{\partial T} \right)_V \tag{6.27}$$

Two general methods are available for evaluating such properties. In the first method we use several simulations to determine values of the simple quantity (E in the case of C_v) as a function of the independent variable (T here). We then compute the response function separately from the simulations, either by numerical differentiation or by analytically differentiating an empirical fit to the simulation results for $E(T)$.

In the second method we evaluate the derivative analytically via statistical mechanics. The analytical form for the derivative always involves a fluctuation; for example, the isometric heat capacity is [2, 3]

$$C_v = \frac{1}{kT^2} \langle (\delta E)^2 \rangle \tag{6.28}$$

where δE is the fluctuation of the internal energy about its average value

$$\delta E = E - \langle E \rangle \tag{6.29}$$

and hence, $\langle(\delta E)^2\rangle$ is the mean-square fluctuation

$$\left\langle(\delta E)^2\right\rangle = \left\langle(E - \langle E\rangle)^2\right\rangle \tag{6.30}$$

We then use simulation to accumulate this mean-square fluctuation and hence, by a relation such as (6.28), we obtain the response function.

Of these two methods, the first is often more accurate than the second, but the first has the disadvantage that several simulations must be done before the derivative can be estimated. The second method produces an estimate for the derivative from a single simulation; however, the derivative itself cannot be evaluated as the simulation proceeds. During a run the average $\langle E\rangle$ is accumulated, and instantaneous values $E(t)$ are stored on disk or tape. Only at the conclusion of the run can we compute the fluctuations needed in (6.30).

We can maneuver around this cumbersome realization of method 2 by expanding the quadratic in (6.30) to obtain the alternative form

$$\left\langle(\delta E)^2\right\rangle = \langle E^2\rangle - \langle E\rangle^2 \tag{6.31}$$

Note that since the lhs is necessarily positive, we must always have $\langle E^2\rangle > \langle E\rangle^2$. The form (6.31) is appealing because it avoids the reanalysis of data required by (6.30): we merely accumulate both the average E and the average E^2 during the run. Unfortunately, (6.31) is often less accurate than (6.30) because of round-off errors—(6.31) suffers from the disease of small difference of large numbers. Aside from these computational details, the relaxation time for fluctuations is generally longer than that for the average quantity itself, and therefore, to obtain reliable results from method 2, long runs with large numbers of particles are needed.

Besides these practical difficulties in using fluctuation expressions, there is a theoretical problem: the relations between response functions and fluctuations depend on the choice of independent variables used to set the thermodynamic state. That is, fluctuation expressions depend on the statistical mechanical ensemble. Thus, the fluctuation expression (6.28) for C_v applies only in a system whose state is specified by fixed values of the number of atoms N, the volume V, and the temperature T; these quantities identify the canonical ensemble in statistical mechanics. In contrast, in the isolated system of molecular dynamics, the total internal energy E does not fluctuate and so C_v cannot be obtained from (6.28).

Most texts in statistical mechanics avoid developing fluctuation expressions in the microcanonical ensemble; instead, fluctuation expressions are developed in some other ensemble, and those results are converted, via Legendre transforms, to the microcanonical ensemble. This is the approach taken by Lebowitz et al. [13] and by Cheung [14]. However, as shown by Pearson et al. [15], one may also start directly in the microcanonical ensemble and develop

all of thermodynamics without appealing to other ensembles. Since the microcanonical ensemble is central to isolated-system molecular dynamics and since the microcanonical ensemble typically receives meager attention in statistical mechanics texts, this direct approach is presented in Appendix C.

Unfortunately, the expressions for response functions obtained in the Legendre transform method differ somewhat from those obtained in the direct method. The two sets of response functions coincide as the number of atoms N is increased [15]; however, in simulations N may not be large. Apparently, the expressions obtained via Legendre transforms are strictly valid only when N is large, while the expressions obtained in the direct method apply for any N. This distinction is likely of little import and must usually be overshadowed by statistical uncertainties in the simulation results.

6.2.1 Isometric Heat Capacity

In Appendix C we show that the isometric heat capacity can be evaluated directly in the microcanonical ensemble, resulting in an expression containing the average reciprocal kinetic energy,

$$C_v^* \equiv \frac{C_v}{Nk} = \left[N - NT^* \left(\frac{3N}{2} - 1 \right) \langle E_k^{*-1} \rangle \right]^{-1} \tag{6.32}$$

Although (6.32) may not appear to involve a fluctuation, recall that T is proportional to the average kinetic energy, and so the rhs of (6.32) essentially involves the fluctuation of $[\langle E_k \rangle \langle E_k^{-1} \rangle]$ about unity.

Alternatively, Lebowitz et al. [13] show how fluctuations in the canonical situation are related to those in a molecular dynamics isolated system; for an isolated system containing spherical molecules, they find

$$C_v^* \equiv \frac{C_v}{Nk} = \frac{3}{2} \left[1 - \frac{2}{3NT^{*2}} \langle (\delta \mathscr{U}^*)^2 \rangle \right]^{-1} \tag{6.33}$$

where $\delta \mathscr{U}$ is the fluctuation in the total configurational internal energy. To maintain constant total energy in an isolated system, the mean-square fluctuations in the configurational energy must equal those of the kinetic energy; hence, (6.33) can also be written as

$$C_v^* = \frac{3}{2} \left[1 - \frac{2}{3NT^{*2}} \langle (\delta E_k^*)^2 \rangle \right]^{-1} \tag{6.34}$$

As N goes large, expressions (6.32) and (6.34) become identical (Exercise 6.17).

Usually the full heat capacity is not what we want; instead, we often need the residual part C_v^R, the part with the ideal-gas contribution removed. For

spheres,

$$C_v^{*R} = C_v^* - \tfrac{3}{2} \tag{6.35}$$

Combining (6.32) and (6.35) produces

$$C_v^{*R} = \frac{-(\frac{3}{2}N-1)\left[1-\frac{3}{2}NT^*\langle E_k^{*-1}\rangle\right]}{N\left[1-(\frac{3}{2}N-1)T^*\langle E_k^{*-1}\rangle\right]} \tag{6.36}$$

while combining (6.33) and (6.35) produces

$$C_v^{*R} = \frac{\langle(\delta\mathscr{U}^*)^2\rangle}{NT^{*2} - \frac{2}{3}\langle(\delta\mathscr{U}^*)^2\rangle} \tag{6.37}$$

We have done calculational tests that compare values for C_v^R obtained from (6.36) and (6.37) and direct evaluation of the derivative (6.27). The tests were done on the Lennard-Jones fluid at $\rho^* = 0.7$. To compute the derivative (6.27), we used for U_c the simulation result given in (6.10); thus, differentiating (6.10) with respect to temperature gives

$$C_v^{*R} = 0.8893 - 0.27176T^* + 0.046779T^{*2} \tag{6.38}$$

which applies over the temperature range $0.96 < T^* < 2.23$. Values of C_v^{*R} computed from this equation are compared in Figure 6.6 with values obtained using the fluctuation expressions (6.36) and (6.37). In using these fluctuation expressions, intermediate averages such as $\langle U\rangle$ and $\langle E_k^{-1}\rangle$ *must* be computed to at least five significant figures. Figure 6.6 shows that the two fluctuation expressions are equally reliable in providing C_v; however, the simple quadratic (6.38) consistently underestimates C_v^R, though it is generally within the statistical uncertainties of the fluctuation results.

In Figure 6.7 the simulation results for C_v^R obtained from (6.37) are compared with values obtained from the Nicolas et al. [4] and Ree [5] correlations. The Ree correlation consistently underestimates C_v^R, while the Nicolas et al. correlation underestimates C_v^R at high temperatures but overestimates it at low temperatures.

6.2.2 Adiabatic Compressibility

The adiabatic compressibility κ_s measures how the system volume responds to a reversible adiabatic (hence, isentropic) change in pressure,

$$\kappa_s = \frac{-1}{V}\left(\frac{\partial V}{\partial P}\right)_s \tag{6.39}$$

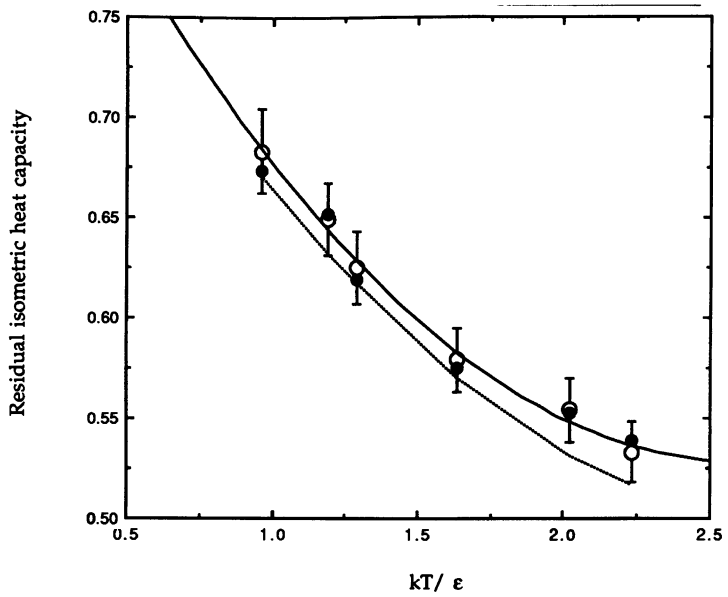

FIGURE 6.6 Comparison of various simulation results for C_v^{*R} for the Lennard-Jones fluid at $\rho\sigma^3 = 0.7$. Open circles were obtained from the fluctuation formula (6.37) involving the internal energy U_c. The error bars on these circles are ± 2 standard deviations for each average. The closed circles were obtained from the fluctuation formula (6.36) involving the reciprocal kinetic energy. The dotted line was obtained from (6.38), the derivative of the empirical fit to U_c. The solid line is a direct fit of a quadratic to the open circles. The simulations are described in Section 6.1.1.

There is no known way to specify a particular value of the entropy S in a molecular dynamics run, and so κ_s cannot be evaluated by numerically estimating the derivative $(\partial V/\partial P)_s$—we are forced to use a fluctuation expression. Fluctuation expressions for κ_s have been obtained directly in the microcanonical ensemble [15] and indirectly from the isothermal compressibility in the canonical ensemble [14]. The latter appears to be easier to implement in simulations, and so we consider only that expression here. Its general form involves pressure fluctuations $\langle(\delta P)^2\rangle$, and for atomic substances it is

$$\kappa_s = \left[\frac{2}{3}P + \rho kT + \langle\theta\rangle - \frac{N}{\rho kT}\langle(\delta P)^2\rangle\right]^{-1} \tag{6.40}$$

where P is the full pressure, as in (6.13). For pairwise additive potentials

$$\theta = \frac{1}{9V}\sum_{i<j} r_{ij}^2 \frac{\partial^2 u(r_{ij})}{\partial r_{ij}^2} \tag{6.41}$$

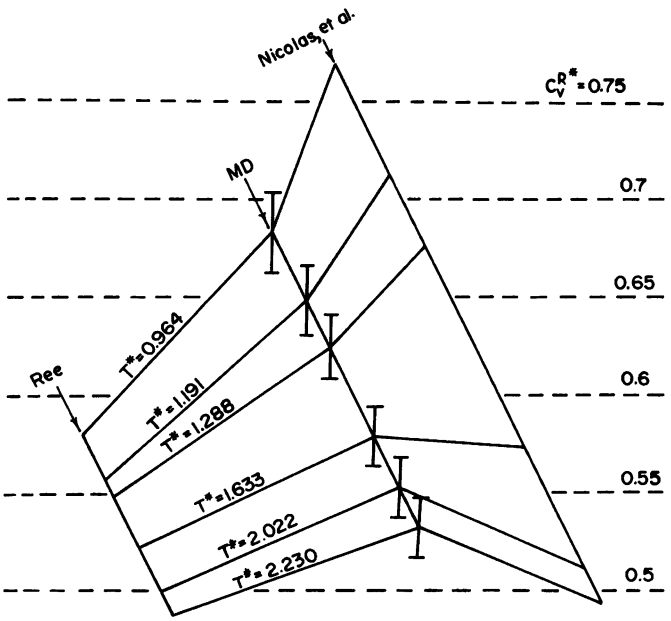

FIGURE 6.7 Tests of Ree and Nicolas et al. equations of state for the residual isometric heat capacity of the Lennard-Jones fluid at $\rho^* = 0.7$. The simulation results shown here are from (6.37), which appear as the open circles in Figure 6.6; the runs are described in Section 6.1.1. The error bars are statistical uncertainties taken to be ± 2 standard deviations of each average.

Moreover, when $u(r)$ is the Lennard-Jones potential, θ simplifies to [16]

$$\langle \theta_{LJ} \rangle = \frac{-8U_c}{V} + \tfrac{19}{3}(P - \rho kT) \tag{6.42}$$

Combining (6.40) and (6.42) gives

$$\kappa_s^* = \frac{\kappa_s \varepsilon}{\sigma^3} = \left[7P^* - \frac{16\rho^* T^*}{3} - 8\rho^* U_c^* - \frac{N}{\rho^* T^*} \langle (\delta P^*)^2 \rangle \right]^{-1} \tag{6.43}$$

Recall that U_c^* is intensive: it is the internal energy per atom.

Sample results obtained from (6.43) for the Lennard-Jones fluid are presented in Figure 6.8. For the states tested, the Nicolas et al. [4] equation gives κ_s within the uncertainties of the simulation results. The Ree [5] correlation is satisfactory at high temperatures but underestimates κ_s at low temperatures.

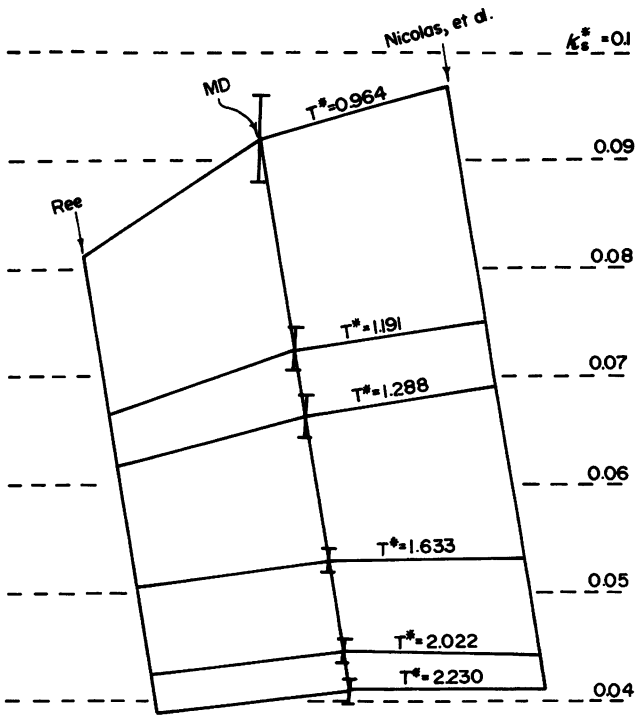

FIGURE 6.8 Tests of Ree and Nicolas et al. equations of state for the adiabatic compressibility κ_s^* of the Lennard-Jones fluid at $\rho^* = 0.7$. The simulation results are from the runs described in Section 6.1.1. The error bars are statistical uncertainties taken to be ± 2 standard deviations of each average.

6.2.3 Thermal Pressure Coefficient

The thermal pressure coefficient γ_v measures how the pressure responds to an isometric change in temperature,

$$\gamma_v = \left(\frac{\partial P}{\partial T}\right)_V \tag{6.44}$$

Like the isometric heat capacity, γ_v can be determined either directly from this definition or from fluctuation expressions [14, 15]. One such expression [14] involves cross-fluctuations in the pressure and kinetic energy $\langle \delta E_k \, \delta P \rangle$,

$$\gamma_v^* \equiv \frac{\gamma_v \sigma^3}{k} = \tfrac{2}{3} C_v^* \left[\rho^* - \frac{1}{T^{*2}} \langle \delta E_k^* \, \delta P^* \rangle \right] \tag{6.45}$$

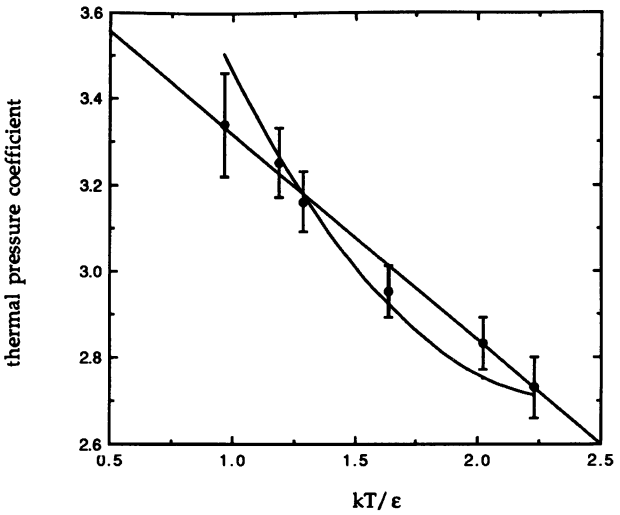

FIGURE 6.9 Comparison of various simulation results for the thermal pressure coefficient γ_v^* of the Lennard-Jones fluid at $\rho\sigma^3 = 0.7$. Points were obtained directly from simulation using the fluctuation formula (6.45). The error bars on these points are statistical uncertainties reported at ± 2 standard deviations of each average. The curved line is the quadratic (6.47), obtained from the derivative of the empirical fit (6.19) to the residual pressure. The straight line is a direct fit to the points. The simulations are described in Section 6.1.1.

where

$$\langle \delta E_k \, \delta P \rangle = \langle (E_k - \langle E_k \rangle)(P - \langle P \rangle) \rangle \tag{6.46}$$

E_k is the extensive kinetic energy, and C_v is the full heat capacity, not just the residual part.

Simulation values of γ_v computed from the derivative (6.44) are compared in Figure 6.9 with values from the fluctuation expression (6.45). The derivative results were obtained by differentiating the simulation results (6.19) for the pressure; that temperature differentiation produces

$$\gamma_v^* = 4.9808 - 1.927T^* + 0.408T^{*2} \tag{6.47}$$

which applies only at $\rho^* = 0.7$ and $0.96 < T^* < 2.23$. The γ_v values obtained from the empiricism (6.47) are generally within the uncertainties of the fluctuation results; however, the curvature of the quadratic (6.47) is clearly wrong at both low and high temperatures. A straight-line fit directly to the

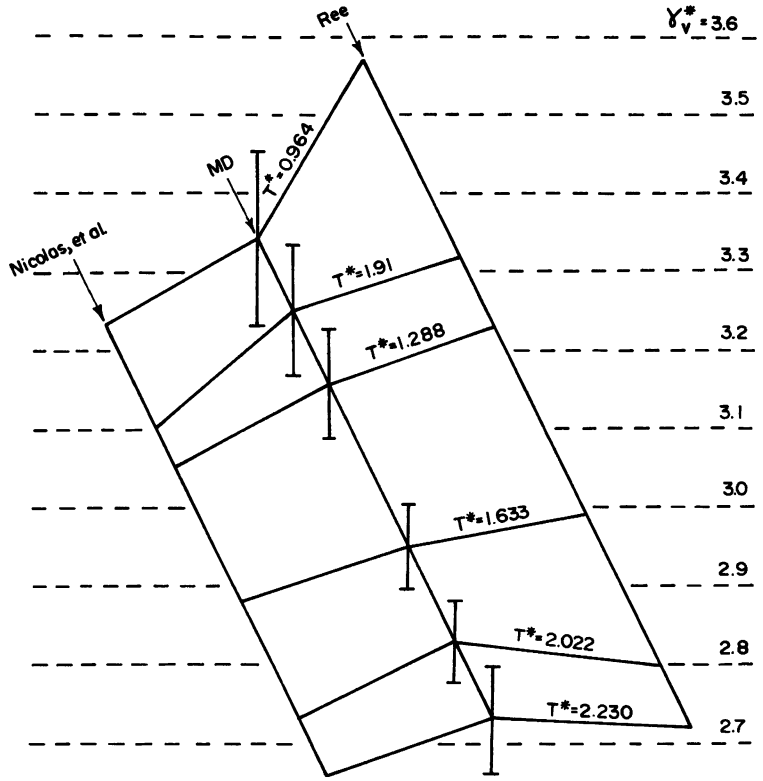

FIGURE 6.10 Tests of Ree and Nicolas et al. equations of state for the thermal pressure coefficient γ_v of the Lennard-Jones fluid at $\rho^* = 0.7$. The simulation results are from the runs described in Section 6.1.1. The error bars are statistical uncertainties taken to be ± 2 standard deviations of each average.

fluctuation results from (6.45) passes within the uncertainties of all the data in the figure.

In Figure 6.10 we use values of γ_v from the fluctuation expression (6.45) to test the Lennard-Jones equations of state [4, 5]. Except at low temperatures, both correlations provide γ_v within the uncertainties of the simulation results. The Nicolas et al. equation consistently underestimates γ_v, while the Ree equation underestimates γ_v at high temperatures and overestimates it at low temperatures.

6.2.4 Other Response Functions

With values for C_v, κ_s, and γ_v obtained from molecular dynamics, all remaining response functions can be evaluated from classical thermodynamic

relations [17] without recourse to further analysis of simulation data. Thus,

$$\gamma = V\left(\frac{\partial P}{\partial E}\right)_V = \frac{V}{C_v}\gamma_v \quad \text{(Grüneisen parameter)} \tag{6.48}$$

$$\kappa_T^{-1} = \left[\frac{-1}{V}\left(\frac{\partial V}{\partial P}\right)_T\right]^{-1}$$

$$= \kappa_s^{-1} - \frac{T}{\rho}\frac{\gamma_v^2}{C_v/N} \quad \text{(isothermal compressibility)} \tag{6.49}$$

$$C_p = \left(\frac{\partial H}{\partial T}\right)_P = \frac{\kappa_T C_v}{\kappa_s} \quad \text{(isobaric heat capacity)} \tag{6.50}$$

$$\beta = \frac{1}{V}\left(\frac{\partial V}{\partial T}\right)_P = \kappa_T \gamma_v \quad \text{(volume expansivity)} \tag{6.51}$$

$$\mu = \left(\frac{\partial T}{\partial P}\right)_H = \frac{V(T\alpha - 1)}{C_p} \quad \text{(Joule–Thomson coefficient)} \tag{6.52}$$

$$w = \sqrt{\frac{1}{\rho m \kappa_s}} \quad \text{(sonic velocity)} \tag{6.53}$$

Here $H = E + PV$ is the enthalpy and m is the atomic mass.

6.3 ENTROPIC PROPERTIES

Of the many problems in molecular simulation, one of the most vexing is determination of entropic properties—the entropy, the Gibbs and Helmholtz free energies, and the chemical potential. The problem is addressed by an extensive literature and in several review papers [18–21]. The difficulty is that unlike the pressure and internal energy, entropic properties cannot be determined directly because they are not defined as time averages over a phase-space trajectory. Instead, they are related to the phase-space volume. Thus, in an isolated system in which N, V, and E are the independent variables, the entropy S is, from (C.5),

$$S = k \ln \Omega$$

In a system in which N, V, and T are independent, the Helmholtz free

energy is

$$A = -kT \ln Q \tag{6.54}$$

and in a system in which N, P, and T are independent, the Gibbs free energy is

$$G = -kT \ln \Delta \tag{6.55}$$

In these equations Ω is the phase-space volume (aka the microcanonical partition function) available to the isolated system, Q is the phase-space volume available to the *NVT* system (the canonical partition function), and Δ is the phase-space volume available to the *NPT* system. Our first problem is to find an expression that gives one of S, G, or A in terms of some time average. We need evaluate only one of S, G, or A from simulation, for then the other two can be obtained from classical thermodynamics.

In an isolated system the entropy of a pure substance is related to other thermodynamic properties by the fundamental equation

$$dS = \frac{dE}{T} + \frac{P}{T} dV - \frac{\mu}{T} dN \tag{6.56}$$

where $\mu = G/N$ is the chemical potential. This equation suggests three routes to the entropy:

(a) manipulate the system energy E at fixed V and N,
(b) manipulate the system volume V at fixed E and N, or
(c) manipulate the number of molecules N at fixed E and V.

Just as in the experimental situation, each of these routes actually provides a *change* in entropy, not an absolute value. Although several schemes have been devised for realizing these routes via simulation, we discuss here only three. The first is *thermodynamic integration*, which may employ both routes (a) and (b). The other two schemes use route (c), in which we are to determine the response of S to a change in N: the *test particle method*, which evaluates the response in the form of a derivative, and the *coupling parameter method*, which evaluates the response in the form of an integral.

6.3.1 Thermodynamic Integration

The simplest methods for evaluating entropic properties are forms of thermodynamic integration. In these methods we determine the temperature, pressure, or density dependence of a simple thermodynamic property and then compute S, A, or G by integrating the appropriate thermodynamic relation. This strategy avoids introducing complicated time averages into a

simulation program at the price of requiring several simulations to obtain one value of an entropic property.

As an example, we can use isolated-system simulations to compute the difference in entropy between two states at the same density (fixed N and V). In each of a series of simulations between the initial and final states (1 and 2), we would accumulate the average temperature and then, at the end of the series, compute ΔS via an integrated form of the fundamental equation (6.56):

$$S(E_2) - S(E_1) = \int_{E_1}^{E_2} \frac{dE}{T} \tag{6.57}$$

Alternatively, we can use temperature rather than total energy as the independent variable; thus, applying the chain rule, (6.57) becomes

$$S(T_2) - S(T_1) = \int_{T_1}^{T_2} \frac{1}{T} \left(\frac{\partial E}{\partial T} \right)_{NV} dT = \int_{T_1}^{T_2} \frac{C_v}{T} dT \tag{6.58}$$

where the integration must be done along a line of constant density (isochore). As an example, (6.38), which gives the temperature dependence of C_v for the Lennard-Jones fluid at $\rho^* = 0.7$, could be used in (6.58) to obtain ΔS.

Similarly, if we want the difference in entropy between two states at the same E and N (the states differ in volume and therefore in density), then the fundamental equation (6.56) gives the effect of a change in density as

$$S(\rho_2) - S(\rho_1) = -\int_{\rho_1}^{\rho_2} \frac{PN}{\rho^2 T} d\rho \quad \text{(fixed } E \text{ and } N\text{)} \tag{6.59}$$

To use (6.59), the total energy must be set to a prechosen value in each of a series of runs. This may be done by using (5.22) to scale the initial velocities.

Instead of (6.59), however, we more often want the difference in entropy between two states at the same T and N; then the fundamental equation (6.56) leads to

$$S(\rho_2) - S(\rho_1) = \frac{1}{T}[E(\rho_2) - E(\rho_1)] - \frac{N}{T} \int_{\rho_1}^{\rho_2} \frac{P}{\rho^2} d\rho \tag{6.60}$$

To use (6.60), we need simulation data for $E(\rho)$ and $P(\rho)$ along an isotherm; call it T_{set}. However, we cannot predetermine exactly the temperature in isolated-system simulations, although by scaling the atomic velocities during an equilibration phase, the final average temperature can be made close (generally within 5%) to the desired value. Call this final computed tempera-

ture T_{cal}. Then by using the heat capacity and thermal pressure coefficient, we can correct the simulation results from $E(\rho, T_{cal})$ and $P(\rho, T_{cal})$ to the needed values $E(\rho, T_{set})$ and $P(\rho, T_{set})$:

$$E(\rho, T_{set}) - E(\rho, T_{cal}) = \int_{T_{cal}}^{T_{set}} C_v \, dT \approx (T_{set} - T_{cal}) C_v(\rho, T_{cal}) \quad (6.61)$$

$$P(\rho, T_{set}) - P(\rho, T_{cal}) = \int_{T_{cal}}^{T_{set}} \gamma_v \, dT \approx (T_{set} - T_{cal}) \gamma_v(\rho, T_{cal}) \quad (6.62)$$

An alternative form of (6.60) is given in Exercise 6.31.

Thermodynamic integration is often the most reliable method for obtaining entropic properties because the integrands can usually be reduced to combinations of simple thermodynamic quantities and because integration tends to be forgiving of small uncertainties in individual contributions to integrands. In spite of its accuracy, thermodynamic integration is not often used because several simulations must be done to obtain one value of ΔS. In view of the ease and low cost of performing simulations, this attitude is largely outdated. As a general rule, we should start simply and leave sophisticated methods until we have experience with our problem. For example, (6.58) and (6.59) require nothing new: we need only run an isolated-system molecular dynamics program several times between the requisite initial and final states. If a simple method gives accurate results, why invest time implementing a sophisticated method? If you are simulating systems involving very large numbers of degrees of freedom, then multiple intermediate simulations may be overly expensive and more sophisticated methods must be considered. Otherwise, thermodynamic integration should be the method considered first.

6.3.2 Test Particle Method

Thermodynamic integration gives changes in entropy resulting from changes in either energy E or volume V; in contrast, the test particle method essentially estimates the change in S that occurs in response to a change in the number of molecules N. For a system of fixed E and V, such a change in S is proportional, according to the fundamental equation (6.56), to the chemical potential

$$\mu = -T\left(\frac{\partial S}{\partial N}\right)_{EV} \quad (6.63)$$

In particular, the chemical potential is related to the reversible work required